

NASA Contractor Report 172527

ICASE REPORT NO. 84-62

NASA-CR-172527
19850011055

ICASE

INSTITUTE FOR COMPUTER APPLICATIONS IN SCIENCE AND ENGINEERING
NASA Langley Research Center, Hampton, Virginia 23665

A MULTISTAGE TIME-STEPPING SCHEME FOR
THE NAVIER-STOKES EQUATIONS

R. C. Swanson

Eli Turkel

Contract No. NAS1-17070
February 1985

INSTITUTE FOR COMPUTER APPLICATIONS IN SCIENCE AND ENGINEERING
NASA Langley Research Center, Hampton, Virginia 23665

Operated by the Universities Space Research Association



National Aeronautics and
Space Administration

Langley Research Center
Hampton, Virginia 23665

LIBRARY COPY

MARK 1 1 1985

LANGLEY RESEARCH CENTER
LIBRARY, NASA
HAMPTON, VIRGINIA

3 1176 00519 3645

**A MULTISTAGE TIME-STEPPING SCHEME FOR THE
NAVIER-STOKES EQUATIONS**

R. C. Swanson
NASA Langley Research Center

Eli Turkel
Tel-Aviv University
and
Institute for Computer Applications in Science and Engineering

Abstract

A class of explicit multistage time-stepping schemes is used to construct an algorithm for solving the compressible Navier-Stokes equations. Flexibility in treating arbitrary geometries is obtained with a finite-volume formulation. Numerical efficiency is achieved by employing techniques for accelerating convergence to steady state. Computer processing is enhanced through vectorization of the algorithm. The scheme is evaluated by solving laminar and turbulent flows over a flat plate and an NACA 0012 airfoil. Numerical results are compared with theoretical solutions or other numerical solutions and/or experimental data.

To be presented at the AIAA 23rd Aerospace Sciences Meeting, Reno, Nevada, January 14-17, 1985, Paper No. 85-0035.

Research was supported by the National Aeronautics and Space Administration under NASA Contract No. NAS1-17070 while the second author was in residence at ICASE, NASA Langley Research Center, Hampton, VA 23665.

Introduction

In recent years, much progress has been made in the development of faster methods for solving the compressible Navier-Stokes equations. This progress is due primarily to improved numerical algorithms and the arrival of specialized computers such as vector processors. However, many more contributions in these areas will be necessary before efficient and reliable solutions of the Navier-Stokes equations can be obtained for complex aerodynamic configurations.

The current availability of a variety of solvers for the Euler equations provides many opportunities for exploring possible Navier-Stokes solvers. One strong candidate for a rapid solver is the very efficient explicit multistage time-stepping scheme for the Euler equations developed by Jameson, Schmidt, and Turkel.¹ This algorithm is formally second-order accurate except near shock waves where the controlled addition of dissipation permits shock capturing without oscillations. It has the highly desirable property that the steady-state solution is independent of the time step. The efficiency and robustness of this finite-volume scheme has been demonstrated by several investigators.²⁻⁴ Also, this scheme has been successfully applied to three-dimensional flow problems.⁵⁻⁶ In the present work, this algorithm is extended to allow the computation of viscous flows. Computational efficiency is achieved for high Reynolds number viscous flows in three ways: 1) use of local time stepping; 2) extension of local stability range by implicit residual smoothing; 3) vectorization of computer code.

While the current effort was in progress, Agarwal and Deese⁷ presented a Runge-Kutta scheme for the thin-layer Navier-Stokes equations. Their principal purpose was to demonstrate the versatility of a Runge-Kutta scheme

by applying it to a variety of fluid dynamics problems. Thus, the focus of their work is quite different from that of the present investigation, where the emphasis is on accuracy and convergence acceleration.

In this paper the governing equations and basic elements of the viscous flow solver are presented. An initial evaluation of the numerical method is achieved by solving laminar and turbulent flows over a flat plate and an NACA 0012 airfoil. Computer results are compared to theoretical solutions or other numerical solutions and/or experimental data. Convergence behavior of the scheme is also discussed.

Governing Equations

Let ρ , (u, v) , p , E , and H denote the density, Cartesian velocity components, pressure, total internal energy, and total enthalpy, respectively. The unsteady, two-dimensional Navier-Stokes equations, neglecting body forces and heat sources, can be written in integral form as follows:

$$\frac{\partial}{\partial t} \iiint_V W dV + \iint_S \bar{H} \cdot \vec{n} dS = 0 \quad (1)$$

where

$$W = \begin{bmatrix} \rho \\ \rho u \\ \rho v \\ \rho E \end{bmatrix} \quad \bar{H} = \begin{bmatrix} \vec{pq} \\ \rho u \vec{q} + p \vec{e}_x + \vec{\tau} \cdot \vec{e}_x \\ \rho v \vec{q} + p \vec{e}_y + \vec{\tau} \cdot \vec{e}_y \\ \hat{\rho} H q + \vec{\tau} \cdot \vec{q} - \vec{Q} \end{bmatrix}$$

$$\vec{q} = u\vec{e}_x + v\vec{e}_y$$

$$\vec{\tau} = \sigma_x \vec{e}_x \vec{e}_x + \tau_{xy} \vec{e}_x \vec{e}_y + \tau_{yx} \vec{e}_y \vec{e}_x + \sigma_y \vec{e}_y \vec{e}_y$$

$$\sigma_x = -\lambda \left(\frac{\partial u}{\partial x} + \frac{\partial v}{\partial y} \right) - 2\mu \frac{\partial u}{\partial x}$$

$$\tau_{xy} = \tau_{yx} = -\mu \left(\frac{\partial u}{\partial y} + \frac{\partial v}{\partial x} \right)$$

$$\sigma_y = -\lambda \left(\frac{\partial u}{\partial x} + \frac{\partial v}{\partial y} \right) - 2\mu \frac{\partial v}{\partial y}$$

$$\vec{Q} = k\nabla T = k \left(\frac{\partial T}{\partial x} \vec{e}_x + \frac{\partial T}{\partial y} \vec{e}_y \right)$$

$$E = e + \frac{1}{2} (u^2 + v^2)$$

$$\hat{H} = E + \frac{p}{\rho}$$

and \vec{e}_x, \vec{e}_y are unit vectors of the Cartesian coordinate system (x, y) , and \vec{n} is a unit vector normal to the surface S enclosing the volume V . In this paper the working fluid is air, and it is assumed to be thermally and calorically perfect. That is, the equation of state is

$$p = \rho RT \quad (2)$$

where $R = \bar{C}_p - \bar{C}_v$, and the specific heats \bar{C}_p, \bar{C}_v are constant. The quantities μ and λ are the first and second coefficients of viscosity, respectively, and λ is taken to be $-\frac{2}{3}\mu$ (Stokes hypothesis). A simple

power law is used to determine μ . The coefficient of thermal conductivity (k) is evaluated using the constant Prandtl number assumption.

Finite-Volume Formulation

In two dimensions the volume has unit depth, and thus Eq. (1) can be written as

$$\frac{\partial}{\partial t} \iint_{\Omega} W dx dy + \int_{\partial\Omega} \bar{\bar{H}} \cdot \vec{n} ds = 0 \quad (3)$$

where Ω is the region of interest, and $\partial\Omega$ is the boundary curve. Let the second-order tensor $\bar{\bar{H}}$ be defined by

$$\bar{\bar{H}} = \vec{F}_x + \vec{G}_y \quad (4)$$

where

$$F = \begin{bmatrix} \rho u \\ \rho u^2 + p + \sigma_x \\ \rho uv + \tau_{xy} \\ \hat{\rho u H} + u \sigma_x + v \tau_{xy} - k \frac{\partial T}{\partial x} \end{bmatrix}$$

$$G = \begin{bmatrix} \rho v \\ \rho uv + \tau_{yx} \\ \rho v^2 + p + \sigma_y \\ \hat{\rho v H} + u \tau_{yx} + v \sigma_y - k \frac{\partial T}{\partial y} \end{bmatrix} .$$

Then, using Cartesian coordinates Eq. (3) becomes

$$\frac{\partial}{\partial t} \iint_{\Omega} W dx dy + \int_{\partial\Omega} (F dy - G dx) = 0. \quad (5)$$

The computational region is partitioned with quadrilaterals, and Eq. (5) is applied to each quadrilateral. This process is equivalent to performing a mass, momentum, and energy balance on each cell. By decoupling the temporal and spatial terms, a systems of ordinary differential equations is obtained. These equations can be solved with a variety of time-stepping schemes.

Applying Eq. (3) to an arbitrary quadrilateral (i.e., ABCD in Fig. 1) and approximating the line integrals with the midpoint rule we obtain

$$\frac{d}{dt} (S_{ij} w_{ij}) + L w_{ij} = 0 \quad (6)$$

where L is a spatial discretization operator, and

$$L w_{ij} = H_{AB} + H_{BC} + H_{CD} + H_{DA}.$$

The components of w_{ij} are now cell-averaged quantities, S_{ij} is the area of the cell ABCD, and the indices (i,j) identify the cell. The vectors H_{AB} , H_{BC} , H_{CD} , H_{DA} represent the fluxes through the sides. For example,

$$H_{BC} = F_{BC} \Delta y_{BC} - G_{BC} \Delta x_{BC} \quad (7)$$

where F_{BC} and G_{BC} are the mean values of F and G on the side BC, and

$$\Delta y_{BC} = y_C - y_B$$

$$\Delta x_{BC} = x_C - x_B.$$

Consider the x-momentum equation. The flux associated with face BC is

$$\begin{aligned} H_{BC} &= (u_{i,j+1/2} \Delta y_{BC} - v_{i,j+1/2} \Delta x_{BC}) (\rho u)_{i,j+1/2} \\ &\quad + p_{i,j+1/2} \Delta y_{BC} + (H_{BC})_{vis} \end{aligned} \quad (8)$$

where

$$(H_{BC})_{vis} = (\sigma_x)_{BC} \Delta y_{BC} - (\tau_{yx})_{BC} \Delta x_{BC}$$

and letting ζ be any cell face quantity,

$$\zeta_{i,j+1/2} = \frac{1}{2} (\zeta_{i,j} + \zeta_{i,j+1}).$$

The first-order derivatives of the viscous terms, $(H_{BC})_{vis}$, are evaluated with Green's theorem. For example,

$$\begin{aligned} (u_x)_{i,j+1/2} &= (u_x)_{BC} = \frac{1}{S_{BC}} \iint_{\Omega'} u_x dx dy \\ &= \frac{1}{S_{BC}} \oint_{\partial\Omega'} u dy, \end{aligned} \quad (9a)$$

$$\begin{aligned}
 (u_y)_{i,j+1/2} &= (u_y)_{BC} = \frac{1}{S_{BC}} \iint_{\Omega'} u_y dx dy \\
 &= - \frac{1}{S_{BC}} \int_{\partial\Omega'} u dx,
 \end{aligned} \tag{9b}$$

where

$$S_{BC} = \frac{1}{2} (s_{i,j} + s_{i,j+1})$$

and $\partial\Omega'$ is the curve $A'B'C'D'$ (see Fig. 1). If the streamwise-like differences associated with the viscous flux quantities are neglected (thin-layer Navier-Stokes assumption), the viscous terms in the flux H_{BC} can be given by

$$\begin{aligned}
 (H_{BC})_{vis} &= \frac{1}{S_{BC}} \left[- \left(\frac{4}{3} \Delta y_{CB}^2 + \Delta x_{CB}^2 \right) \right. \\
 &\quad \cdot \mu_A (u_{i,j+1} - u_{i,j}) \\
 &\quad + \left(\frac{1}{3} \Delta y_{CB} \Delta x_{CB} \right) \\
 &\quad \left. \cdot \mu_A (v_{i,j+1} - v_{i,j}) \right], \tag{10}
 \end{aligned}$$

where $\Delta y_{CB} = -\Delta y_{BC}$, $\Delta x_{CB} = -\Delta x_{BC}$, and $\mu_A = \frac{1}{2} (\mu_{i,j} + \mu_{i,j+1})$. Note that with the thin-layer assumption, there are viscous contributions to fluxes H_{BC} and H_{DA} only. In the present work the thin-layer assumption is applied. For additional details on the finite-volume formulation just described, see Ref. 8.

Dissipative Terms

In order to suppress any odd-even point decoupling in the numerical solution and to prevent oscillations in the vicinity of shock waves and stagnation points, artificial dissipation terms are added to the finite-volume scheme. Therefore, Eq. (6) is replaced by

$$\frac{d}{dt} (SW) + LW - DW = 0 \quad (11)$$

where D is the artificial dissipation operator, and the indices have been suppressed for convenience. Through numerical experiments Jameson¹ established that an effective form for DW is a blend of second and fourth differences with coefficients that depend on the local pressure gradient. This form is constructed in the following way:

$$DW = D_x W + D_y W \quad (12)$$

where $D_x W$ and $D_y W$ are the contributions associated with the two coordinate directions, and in conservation form

$$D_x W = d_{i+1/2,j} - d_{i-1/2,j} \quad (13a)$$

$$D_y W = d_{i,j+1/2} - d_{i,j-1/2} \cdot \quad (13b)$$

The terms on the right side of Eqs. (13a) and (13b) have a similar form; for example, taking Δt as the Courant-Friedrichs-Lowy time step,

$$d_{i+1/2,j} = \frac{s_{i+1/2,j}}{\Delta t} \left[\epsilon_{i+1/2,j}^{(2)} (w_{i+1,j} - w_{i,j}) \right. \\ \left. - \epsilon_{i+1/2,j}^{(4)} (w_{i+2,j} - 3w_{i+1,j} + 3w_{i,j} - w_{i-1,j}) \right]. \quad (14)$$

The coefficients $\epsilon^{(2)}$ and $\epsilon^{(4)}$ are adapted to the flow and are defined as follows:

$$\nu_{i,j} = \frac{|p_{i+1,j} - 2p_{i,j} + p_{i-1,j}|}{p_{i+1,j} + 2p_{i,j} + p_{i-1,j}}, \quad (15)$$

$$\epsilon_{i+1/2,j}^{(2)} = \kappa^{(2)} \max(\nu_{i+1,j}, \nu_{i,j}), \quad (16)$$

$$\epsilon_{i+1/2,j}^{(4)} = \max(0, (\kappa^{(4)} - \epsilon_{i+1/2,j}^{(2)})), \quad (17)$$

where typical values of the constants $\kappa^{(2)}$ and $\kappa^{(4)}$ are $1/4$ and $1/256$, respectively. In the current work ρH is used instead of ρE in the dissipative terms in the energy equation. This is done so that constant H can be a solution of the energy equation.

In smooth regions of the flow field, the dissipative terms are third-order. The dissipation becomes first-order in the neighborhood of a shock wave. However, this does not compromise the global second-order accuracy of the finite-volume scheme. Note that the fourth difference is eliminated near shocks since it can have a destabilizing effect on a numerical calculation.⁹

In the case of viscous flows significant gradients in the velocity field exist in the region adjacent to a solid boundary. Therefore, even though the

artificial viscosity coefficients ($\kappa^{(2)}, \kappa^{(4)}$) are small, the artificial dissipation can produce viscous-like effects of the same order as the physical ones. In the present work numerical experiments for turbulent flow over a flat plate showed significant artificial viscous effects, even with $\kappa^{(2)} = 0$ and small values of $\kappa^{(4)}$. By setting the normal contribution to the artificial dissipation ($D_y W$) to zero in at least the law-of-the-wall region of the turbulent boundary layer accurate solutions were obtained (see Results and Discussion section).

Time-Stepping Scheme

A member of a class of four-stage schemes is employed to advance the solution of Eq. (11) in time. This scheme takes the following form at time level n :

$$\begin{aligned} W^{(0)} &= W^n \\ W^{(1)} &= W^{(0)} - \alpha_1 \Delta t R W^{(0)} \\ W^{(2)} &= W^{(0)} - \alpha_2 \Delta t R W^{(1)} \\ W^{(3)} &= W^{(0)} - \alpha_3 \Delta t R W^{(2)} \\ W^{(4)} &= W^{(0)} - \Delta t R W^{(3)} \\ W^{n+1} &= W^{(4)} \end{aligned} \tag{18}$$

where on the $(q+1)$ st stage

$$R_W^{(q)} = \frac{1}{S} (L_W^{(q)} - D_W^{(0)})$$

and

$$\alpha_1 = 1/4, \quad \alpha_2 = 1/3, \quad \alpha_3 = 1/2.$$

For efficiency both the physical and artificial viscous terms are evaluated at the first stage and frozen for the remaining stages. The scheme of Eq. (18) is a modified version of the classical fourth-order Runge-Kutta scheme. The advantage of the modified scheme is that it requires less storage of array quantities in computer processing, an important consideration for three-dimensional calculations. According to linear stability analysis on a model wave equation the modified algorithm has the same stability (i.e., same amplification factor) as the classical scheme.⁵ The method of Eq. (18) is fourth-order accurate in time only for linear equations; it is second-order accurate for nonlinear equations. However, since the primary objective here is to compute steady-state solutions, this is not viewed as a deficiency of the scheme.

The Runge-Kutta time-stepping scheme is more efficient than explicit schemes such as unsplit MacCormack and leapfrog.¹ Also, this scheme has the desirable property that if $R_W^n = 0$, then $w^{(1)} = w^{(0)}$, and thus at the final stage of the scheme $w^{n+1} = w^n$. Therefore, the steady-state solution is independent of the time step, and the scheme is amenable to a variety of techniques for accelerating steady-state convergence.

Acceleration Techniques

Three methods are employed to accelerate convergence of the basic time-stepping scheme. These techniques are as follows: 1) local time stepping; 2) enthalpy damping; 3) residual smoothing. They are discussed in the subsequent subsections.

Local Time Stepping

With this technique the solution is advanced in time with a time step dictated by the local stability limit. In the present work the local Δt is based on the Courant-Friedrichs-Lowy (CFL) stability limit. Local time stepping allows faster signal propagation, and thus faster convergence.

Enthalpy Damping

In Ref. 1 enthalpy damping was introduced for the Euler equations. This method accelerates convergence through artificial damping terms. These terms are added to each equation in general and depend on the deviation of the local total enthalpy (\hat{H}) from the steady-state value (\hat{H}_∞). Since the total enthalpy is constant throughout a steady, inviscid flow field in which uniform free-stream conditions exist, such forcing terms are zero in the steady state.

Under certain assumptions the total enthalpy may be taken as constant for viscous flows. If the dominant viscous terms are retained (boundary-layer type approximation), the following form of the energy equation for laminar flow can be derived:

$$\begin{aligned} \frac{\partial}{\partial t} (\rho E) + \frac{\partial}{\partial x} (\rho u \hat{H}) + \frac{\partial}{\partial y} (\rho v \hat{H}) \\ = \frac{\partial}{\partial y} \left[\frac{\mu}{Pr} \left(\frac{\partial}{\partial y} (\hat{H}) - (1 - Pr) \frac{\partial}{\partial y} \left(\frac{u^2}{2} \right) \right) \right]. \end{aligned} \quad (19)$$

Then, if there is no heat transfer at solid surfaces, and the Prandtl number (Pr) is unity, constant \hat{H} is a steady-state solution of Eq. (19). In the case of turbulent flow a mean flow energy equation of the same form as Eq. (19) can be obtained if the eddy viscosity hypothesis is used (see section on turbulence modeling), and small work terms are neglected. Then, if the surfaces are adiabatic, and both the laminar and turbulent Prandtl numbers are unity, constant total enthalpy is a solution of the energy equation.

Using enthalpy damping computations exhibit a more monotone convergence to steady state. This property is especially useful if an acceleration procedure such as residual smoothing is applied with the Runge-Kutta scheme.

Residual Smoothing

Residual smoothing was first introduced by Lerat¹⁰ for use with the Lax-Wendroff scheme. Jameson¹¹ later introduced a similar technique in conjunction with the Runge-Kutta schemes. With this technique the stability range of the basic time-stepping scheme is extended. Linear stability analysis indicates that the Runge-Kutta scheme with residual smoothing is unconditionally stable if the smoothing parameter is sufficiently large.⁹ However, as revealed in the subsequent analysis, the fastest convergence to steady state is not realized with a very large time step.

Consider the following two-step scheme:

$$\begin{aligned} u^{(1)} &= u^n - \alpha \Delta t L u^n \\ u^{(2)} &= u^n - \Delta t L u^{(1)} \end{aligned} \tag{20}$$

where L is a spatial discretization operator. The residual smoothing for the second stage is given by

$$\prod_{\ell} \left(1 - \frac{\beta_{\ell}}{4} \delta_{xx}^{(\ell)} \right) \left(u^{n+1} - u^n \right) = u^{(2)} - u^n \tag{21}$$

where δ_{xx} is the standard central difference operator, and the product is over the number of space dimensions. Now, consider the model problem

$$u_t + u_x + \epsilon \Delta x^3 u_{xxxx} = 0. \tag{22}$$

If $\epsilon = 0$, a Fourier transform of Eq. (21) yields

$$\begin{aligned} 1 + \beta \sin^2 \frac{\theta}{2} (G - 1) \\ = -i\lambda \sin \theta - \alpha \lambda^2 \sin^2 \theta \end{aligned} \tag{23}$$

where

$$\lambda = \frac{\Delta t}{\Delta x}, \quad \theta = k_x \Delta x$$

and k_x is a wave number. Equation (23) can be written as

$$G = 1 - \frac{i\lambda \sin \theta + \alpha \lambda^2 \sin^2 \theta}{1 + \beta \sin^2 \frac{\theta}{2}}. \quad (24)$$

Then, taking the smoothing parameter $\beta = \sigma \lambda^2$, Eq. (24) for large λ reduces to

$$G(\theta) \approx 1 - \frac{\alpha}{\sigma} \frac{\sin^2 \theta}{\sin^2 \frac{\theta}{2}}. \quad (25)$$

Thus, without an artificial viscosity the highest frequency, $\theta = \pi$, is not damped.

If the artificial third-order dissipation ($\epsilon \neq 0$) is added, then Eq. (24) is replaced by

$$G(\theta) = 1 + \frac{\lambda \tilde{A}(1 + \lambda \tilde{A})}{1 + \sigma \lambda^2 \sin^2 \frac{\theta}{2}} \quad (26)$$

where

$$\tilde{A} = -i \sin \theta + v \sin^4 \frac{\theta}{2}$$

and v is proportional to ϵ . As λ gets large,

$$G(\pi) \sim 1 + \frac{v^2}{\sigma} > 1. \quad (27)$$

Therefore, the scheme is not stable for large λ . However, if the same artificial viscosity is used at both stages, then Eq. (24) is replaced by

$$G(\theta) = 1 - \frac{i\lambda \sin \theta(1 + \alpha \lambda \tilde{A}) - \lambda v \sin^4 \frac{\theta}{2}}{1 + \sigma \lambda^2 \sin^2 \frac{\theta}{2}}. \quad (28)$$

As λ approaches infinity, the coefficient of the artificial viscosity goes to zero, and so Eq. (25) is recovered. When the artificial viscosity term is

frozen, the scheme remains unconditionally stable. However, when λ is large, the highest frequency is damped only a small amount proportional to $1/\lambda$. Therefore, the strategy is to minimize G^*G rather than choose λ large.

The analysis just given for a two-stage time-stepping scheme suggests that for multistage schemes residual smoothing is needed only at alternate stages (i.e., after stages 2 and 4 of a four-stage scheme). This frequency of smoothing has been used in solving the Euler equations. However, based on stability considerations for parabolic problems,⁹ the residual smoothing is applied at every stage in the present scheme for the Navier-Stokes equations.

Boundary Conditions

A typical domain for a viscous airfoil calculation is considered in describing the boundary conditions. At the body surface the boundary conditions are as follows: 1) no slip (velocity components u and v are zero); 2) adiabatic surface condition ($\partial T / \partial y = 0$). The reduced normal momentum equation $\partial p / \partial y = 0$ is used to compute the surface pressure. At the outer boundary (ABC in Fig. 2) both inflow and outflow can occur. Subsonic inviscid characteristic theory indicates that three quantities should be specified at an inflow boundary. In the case of inflow the total enthalpy (\hat{H}), entropy (s), and tangential velocity (U) are assigned free-stream values. A one-dimensional flow analysis is applied normal to the boundary, and the normal velocity (V) is then computed by extrapolating the Riemann invariant

$$V + \frac{2a}{\gamma-1} \quad (29)$$

from the interior of the domain. The quantity a is the speed of sound, and γ is the ratio of specific heats. In the case of outflow the quantities \hat{H} , s , and U are extrapolated from the interior, and the Riemann invariant is

$$V_\infty = \frac{2a_\infty}{\gamma-1} . \quad (30)$$

Two methods have been investigated for treating the downstream (outflow) boundary AC. They are as follows: 1) static pressure is specified, ($p = p_\infty$), and density and velocity components (u, v) are extrapolated from the interior; 2) dependent variables (W) extrapolated from the interior. In the airfoil cases considered, method 2 required less steps for a converged solution than method 1, and the solution in the vicinity of the airfoil was essentially the same. However, method 2 is not consistent with characteristic analysis. At the present time nonreflecting-type boundary conditions are being investigated.

For supersonic flows free-stream conditions are specified at inflow boundaries, and flow quantities are extrapolated from the interior at outflow boundaries.

Turbulence Modeling

Using mass-averaged variables¹² the time-averaged flow equations have the same form as their laminar flow counterparts, except that the stress tensor is augmented by the Reynolds stress tensor, the heat flux vector is augmented by the additional heat flux terms associated with the turbulence, and additional mean energy dissipation terms appear (in many cases these terms can be

neglected). To close the time-averaged equations for turbulent flow the eddy hypothesis (Reynolds stress and heat flux terms are related to mean flow-field gradients) is used. Moreover, the eddy viscosity, which is added to the molecular viscosity to obtain the effective viscosity, is computed with the two-layer algebraic model of Baldwin and Lomax.¹³ The Reynolds heat flux terms are approximated using the constant Prandtl number assumption. Thus,

$$\mu = \mu_l + \mu_t \quad (31a)$$

$$k = \overline{C}_p \left[\left(\frac{\mu}{Pr} \right)_l + \left(\frac{\mu}{Pr} \right)_t \right] \quad (31b)$$

where the subscripts l and t refer to laminar and turbulent. In the present work the Prandtl numbers are assumed to be 1.0.

Results and Discussion

The numerical scheme described in the preceding sections has been applied to the following test problems: 1) flow over a flat plate; 2) flow over an NACA 0012 airfoil. For each test problem, solutions were obtained for both laminar and turbulent flow. In the laminar cases the free-stream Mach number (M_∞) was 0.5, and the free-stream Reynolds number (Re_∞) was 5×10^3 . In the turbulent cases the range of M_∞ was 0.5 - 0.756, and the range of Re_∞ was $10^6 - 4.01 \times 10^6$. The reference length for the airfoil cases was the chord C .

Flat Plate Boundary-Layer Flows

For the flat plate calculations the nondimensional distance between the leading edge ($X/L = 0$) and the downstream boundary of the rectangular computational domain was 1. The upper boundary of the computational domain was at 10δ , where δ was the boundary-layer thickness at the downstream boundary. In the laminar flow case the grid consisted of 60×40 cells. The cell spacing in streamwise direction on the plate was 0.05, and the minimum cell height in the normal direction was 10^{-3} . The grid points were distributed according to a geometric progression in the normal direction. A 60×60 cell grid was used in the turbulent case (same spacing as laminar case in streamwise direction). The normal distance from the plate to the first cell center was $5 \times 10^{-5} L$, which corresponded to a y^+ value of about 2 ($y^+ = y u_\tau / v$, u_τ is the local friction velocity and v is the kinematic viscosity coefficient).

Results for laminar flow over a flat plate are presented in Figs. 3a and 3b. The present computed solution is compared with the incompressible boundary-layer solution of Blasius. Figure 3a shows the variation of skin friction (C_f) with local Reynolds number (Re_x). Note that no attempt has been made to resolve the leading edge region of the plate. This probably accounts for the differences in the skin friction distributions. Although not shown, the predicted velocity profiles are essentially self-similar beyond the initial region (roughly $0 < X/L < 0.225$) of the flat plate. There is reasonably good agreement between a representative velocity profile ($X/L = 0.875$) and the Blasius result (Fig. 3b).

In Figs. 4a - 4c results for turbulent flow over a flat plate are presented. The variation of C_f with Re_x is displayed in Fig. 4a. The

numerical prediction exhibits fairly good agreement with the empirical curve fit ($M_\infty \approx 0$) once fully developed turbulent flow is realized. Figure 4b compares solutions for the velocity profile at $X/L = 0.875$, which were calculated with the following: 1) 1/7-th-power law; 2) Steger Navier-Stokes code¹⁴ (Beam and Warming implicit scheme); 3) present Runge-Kutta code. Both of the numerical results were obtained with the Baldwin-Lomax eddy viscosity model, and they show excellent agreement. The same grid was used in the calculations. Figure 4c compares the computed law of the wall and a curve fit for the experimental data of several investigators¹⁵.

NACA 0012 Airfoil Flows

A typical grid for an airfoil calculation is displayed in Fig. 5. This C-type grid was generated with an algebraic procedure developed by Le Balleur.¹⁶ In the direction approximately perpendicular to the airfoil, the coordinate lines are parabolas intersecting the airfoil and outer boundary at predetermined locations. The second family of coordinate lines were determined by distributing points along the parabolas in accordance with a prescribed function. Additional information concerning grid generation can be obtained from Ref. 16. For all "C" grids used herein the outer boundary was located 5 to 6 chords from the airfoil in all directions. In the laminar flow case, calculations were done on meshes with 128×32 cells and 128×64 cells. The cell spacing in the streamwise direction over the central part of the airfoil was $\Delta X/C = 0.05$. The minimum cell height in the normal-like direction for these grids was about 3×10^{-4} chords and 6×10^{-4} chords, respectively. For turbulent flow computations (120×50 cell grid) the

distance from the airfoil surface to the first cell center was approximately 5×10^{-5} chords. The chordwise spacing at the midsection of the airfoil was $\Delta X/C = 0.036$.

Figures 6a - 6c show results for the laminar flow ($M_\infty = 0.5$, $Re_\infty = 5 \times 10^3$) computation on the 128×64 cell grid. In Fig. 6a the pressure distribution for the viscous flow is compared with that obtained by solving the Euler equations. The presence of strong viscous effects is evident over the aft section of the airfoil. Moreover, as indicated in Fig. 6b, the flow separates at $X/C \approx 0.817$. The size of the thin recirculation region is indicated in the plot of streamlines in Fig. 6c. Since the velocity of the flow is very small in this thin region, the accuracy of the solution there is of special concern. The solution on the 128×64 cell grid was compared with that on a 128×32 cell grid, where the mesh spacing in the normal-like direction is about a factor of 2 larger. These solutions are essentially the same except in the reverse flow region. A bubble that is slightly larger in longitudinal extent (approximately 7 percent larger) is predicted with the finer grid.

Results for subsonic, turbulent flow over the airfoil at zero angle of attack are presented in Figs. 7a - 7c. Figure 7a shows a comparison of the calculated pressure distribution with experimental data.¹⁷ In Fig. 7b the predicted skin friction distribution is compared with that obtained with a boundary-layer code.¹⁸ For the boundary-layer calculation a very fine mesh spacing (more than an order of magnitude smaller than that in the present calculation) was used at the surface, and 100 points were placed across the boundary layer. Since the viscous-inviscid interaction effects are small for this flow, a single pass computation was done. The pressure distribution from

the thin-layer Navier-Stokes solution was prescribed. There is fairly good agreement except at the leading edge, where the present solution does not have adequate resolution for the very thin turbulent boundary layer. In Fig. 7c pressure contours for this case are displayed.

Computed pressure distributions for subsonic ($M_\infty = 0.5$), viscous flow over the airfoil at two angles of attack (1.77 degrees and 3.51 degrees) are compared with those for inviscid flow and with experimental data in Figs. 8 and 9. In each case the angle of attack (α) has been corrected for wind tunnel wall effects. There is good agreement between the present Navier-Stokes results and experiment. The influence of viscosity on these solutions, in particular at the suction peak, is evident.

In Figs. 10a and 10b results for supercritical flow ($M_\infty = 0.756$) and zero angle of attack are presented. The pressure distributions from the viscous and inviscid calculations show good agreement with the data. The supersonic region of the flow is indicated by the Mach number contours in Fig. 10b.

Convergence

For all computations in this paper the flow field was initialized with free-stream conditions. Moreover, the calculations were started impulsively by suddenly introducing the body into a uniform flow and immediately enforcing the appropriate boundary conditions at its surface. To measure convergence the root mean square of the residual of the continuity equation was used. In Fig. 11 convergence histories are shown for the laminar airfoil case on a 128×32 cell grid. For the history labeled A the local CFL number was

2, and enthalpy damping was used. For the history labeled B the CFL number was 6, and both enthalpy damping and residual smoothing were used. These results indicate that satisfactory convergence for engineering applications is achieved in 1300 time steps, which corresponds to 2.5 minutes on the Vector Processing System (VPS) 32 at Langley Research Center. Figures 12a and 12b show residual histories for the zero angle of attack, subcritical, turbulent airfoil case. In Fig. 12a the convergence history, which is highly oscillatory in character, is for a calculation using only local time stepping to accelerate convergence. As seen in Fig. 12b, a computation using enthalpy damping and residual smoothing (CFL number of 5) exhibits much more monotonic convergence behavior. In this case acceptable convergence is realized in about 1250 time steps (4 minutes on the VPS 32). Note that the present computer code is not optimized for the VPS 32 system. With optimization the computer processing times can be reduced by a factor of 2 to 3.

The final rate of reduction of the residual for the turbulent flow cases is quite slow. Based on previous work with Euler equations⁵, significant improvement in this rate appears to be possible with a multigrid scheme. At the present time this is being investigated.

Concluding Remarks

A finite-volume scheme for numerical integration of the Euler equations has been extended to allow solution of the Navier-Stokes equations. The new procedure, which is based on a class of four stage Runge-Kutta time-stepping schemes, has been made numerically efficient through the following convergence acceleration techniques: 1) local time stepping; 2) enthalpy damping; 3)

residual smoothing. Also, the high degree of vectorization possible with the algorithm has yielded an efficient program for vector processors. The scheme has been evaluated by solving the thin layer form of the Navier-Stokes equations for laminar and turbulent flows over a flat plate and an NACA 0012 airfoil. Numerical results have compared well with either theoretical or other numerical solutions and/or experimental data.

References

¹Jameson, A., Schmidt, W., and Turkel, E.: "Numerical Solutions of the Euler Equations by Finite Volume Methods Using Runge-Kutta Time-Stepping Schemes," AIAA Paper 81-1259, June 1981.

²Schmidt, W., Jameson, A., and Whitfield, D.: "Finite Volume Solution for the Euler Equation for Transonic Flow Over Airfoils and Wings Including Viscous Effects," AIAA Paper 81-1265, June 1981.

³Salas, M. D., Jameson, A., and Melnik, R. E.: "A Comparative Study of the Nonuniqueness Problem of the Potential Equation," AIAA Paper 83-1888, July 1983.

⁴Deese, J. E. and Agarwal, R. K., "Calculation of Axisymmetric Inlet Flowfield Using the Euler Equations," AIAA Paper 83-1853, July 1983.

⁵Jameson, A. and Baker, T. J., "Solution of the Euler Equations for Complex Configurations," AIAA Paper 83-1929, July 1983.

⁶Agarwal, R. K. and Deese, J. E.: "Transonic Wing-Body Calculations Using Euler Equations," AIAA Paper 83-0501, January 1983.

⁷Agarwal, R. K. and Deese, J. E.: "Computation of Transonic Viscous Airfoil, Inlet, and Wing Flowfields," AIAA Paper 84-1551, June 1984.

⁸Peyret, R. and Taylor, T. D.: Computational Methods for Fluid Flow,
Springer Series in Computational Physics, Springer-Verlag, 1983.

⁹Turkel, E.: "Acceleration to a Steady State for the Euler Equations," NASA
CR-172398 and ICASE Report No. 84-32, July 1984.

¹⁰Lerat, A.: "Une classe de schémas aux
différences implicites pour les systèmes hyperboliques de lois de
conservation," Comptes Rendus Acad. Sciences Paris, Vol. 288A, 1979.

¹¹Jameson, A.: "The Evolution of Computational Methods in Aerodynamics," J.
Appl. Mech., Vol. 50, 1983.

¹²Rubesin, M. W. and Rose, W. C.: "The Turbulent Mean-Flow, Reynolds-Stress,
and Heat-Flux Equations in Mass-Averaged Dependent Variables," NASA TM
X-62,248, March 1973.

¹³Baldwin, B. S. and Lomax, H.: "Thin Layer Approximation and Algebraic Model
for Separated Turbulent Flows," AIAA Paper 78-257, January 1978.

¹⁴Steger, J. L.: "Implicit Finite Difference Simulation of Flow About
Arbitrary Geometries with Application to Airfoils," AIAA Paper 77-665,
June 1977.

¹⁵Hinze, J. O.: Turbulence, 2nd edition, McGraw-Hill Book Company, Inc., New
York, 1975.

¹⁶Le Balleur, J. C.: "Strong Matching Method for Computing Transonic Viscous Flows Including Wakes and Separations - Lifting Airfoils," La Recherche Aerospatiale (English edition), No. 1981-3.

¹⁷Thibert, J. J., Granjacques, M., and Ohman, L. H.: NACA 0012 Airfoil, AGARD Advisory Report No. 138, Experimental Data Base for Computer Program Assessment, May 1979.

¹⁸Miner, E. W., Anderson, E. C., and Lewis, C. H.: "A Computer Program for Two-Dimensional and Axisymmetric Nonreacting Perfect Gas and Equilibrium Chemically Reacting Laminar, Transitional, and/or Turbulent Boundary Layer Flows," VPI-E-71-8, May 1971 (available as NASA CR-132601).

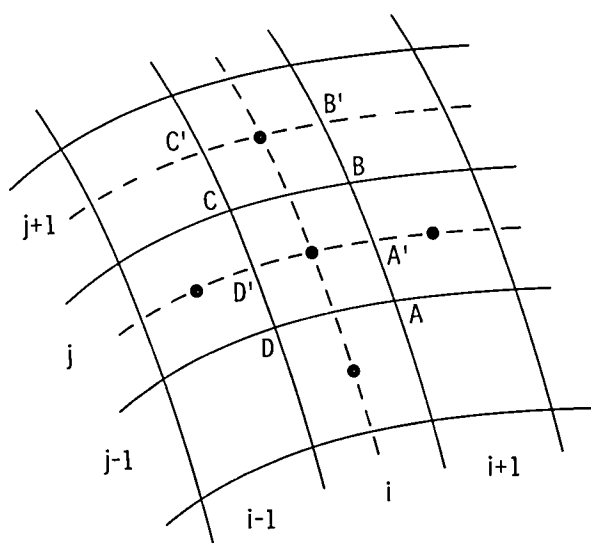


Figure 1. Finite-volume mesh.

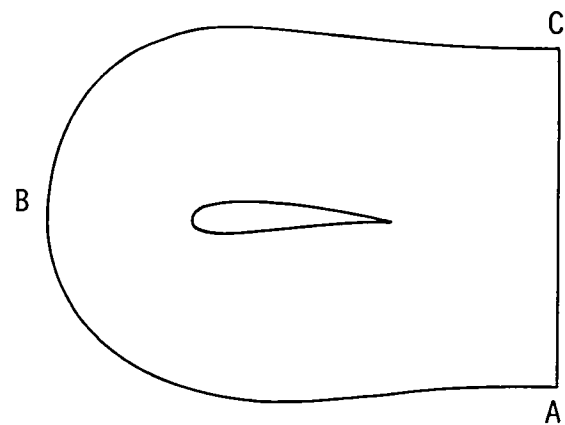
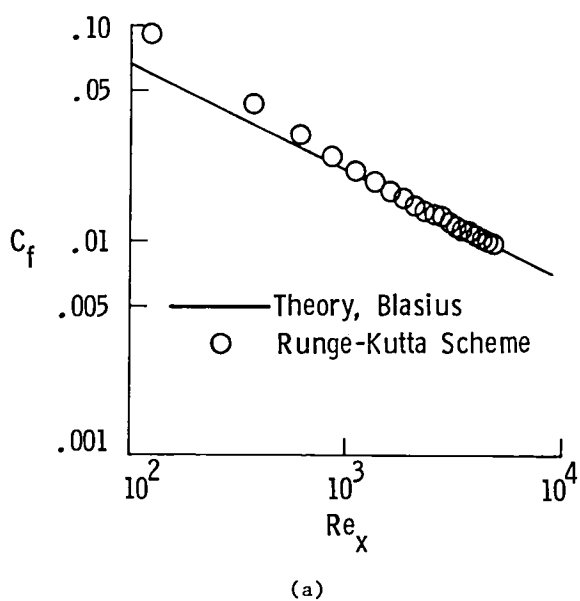
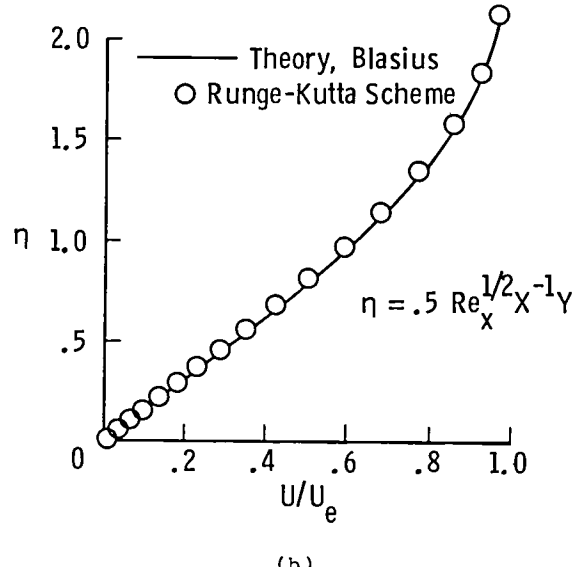


Figure 2. Computational domain for airfoil calculations.



(a)

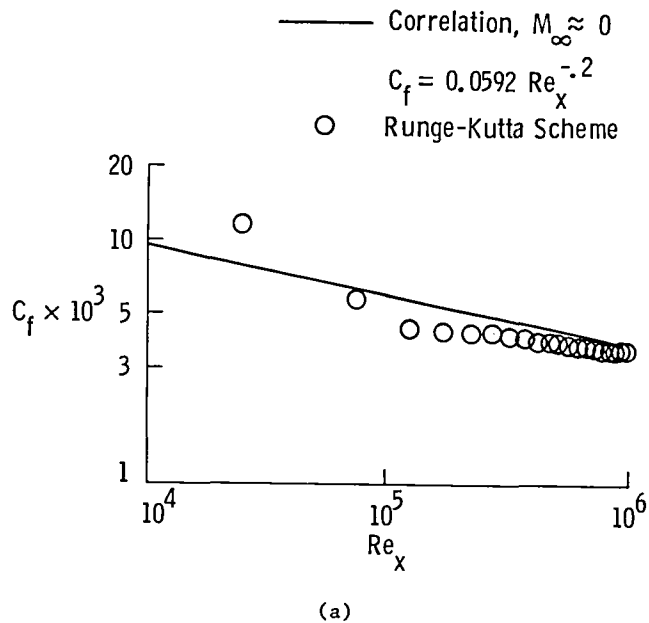


(b)

Figure 3. Laminar flat plate flow:

(a) comparison of skin-friction distributions;

(b) comparison of velocity profiles ($M_\infty = 0.5$, $Re_\infty = 5 \times 10^3$).



(a)

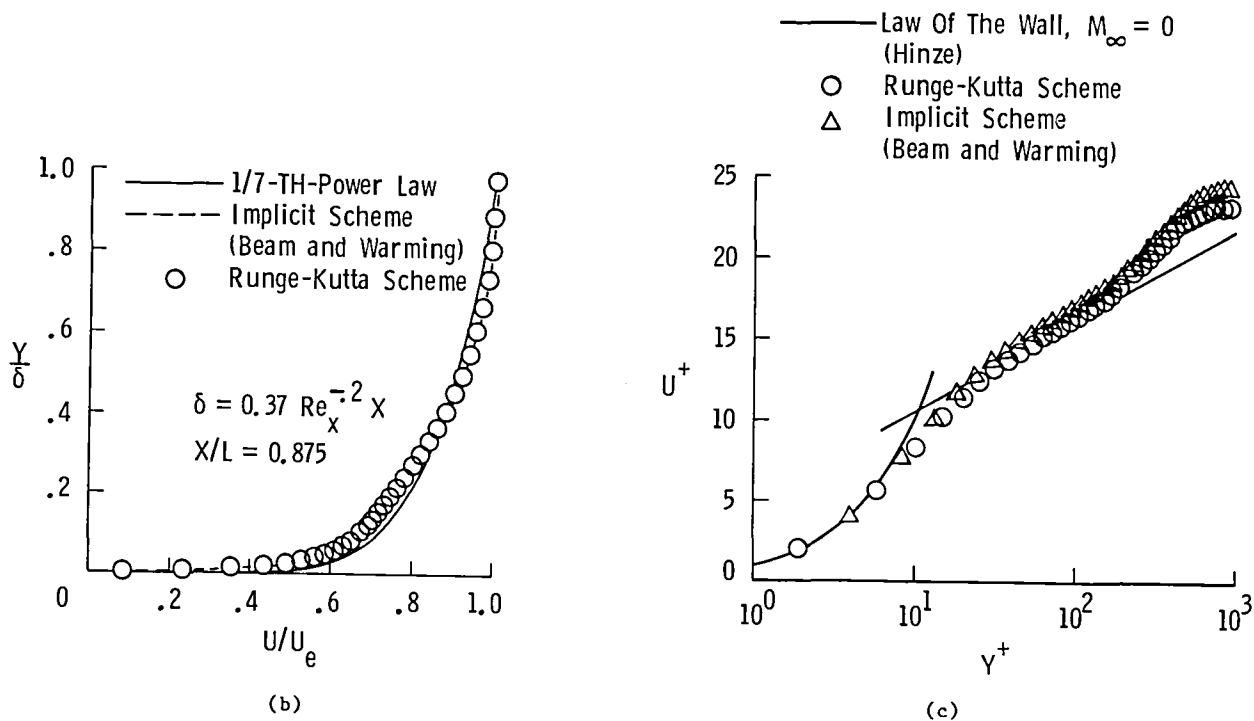


Figure 4. Turbulent flat plate flow:

- (a) comparison of skin friction distributions;
- (b) comparison of velocity profiles;
- (c) comparison of near wall velocity profiles
($M_\infty = 0.5$, $Re_\infty = 10^6$).

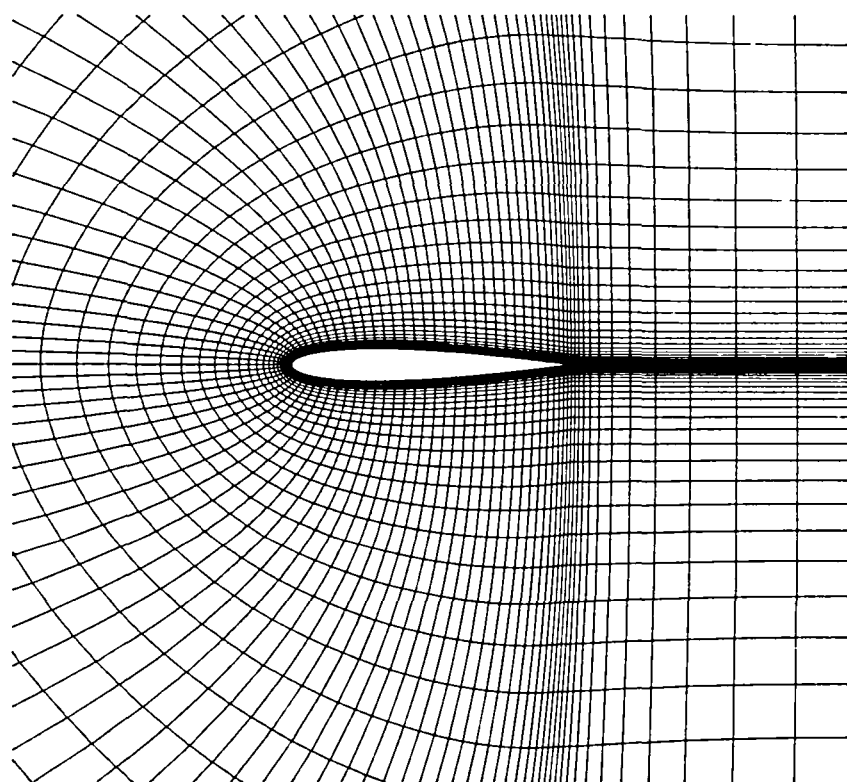


Figure 5. Partial view of typical grid for airfoil calculations.

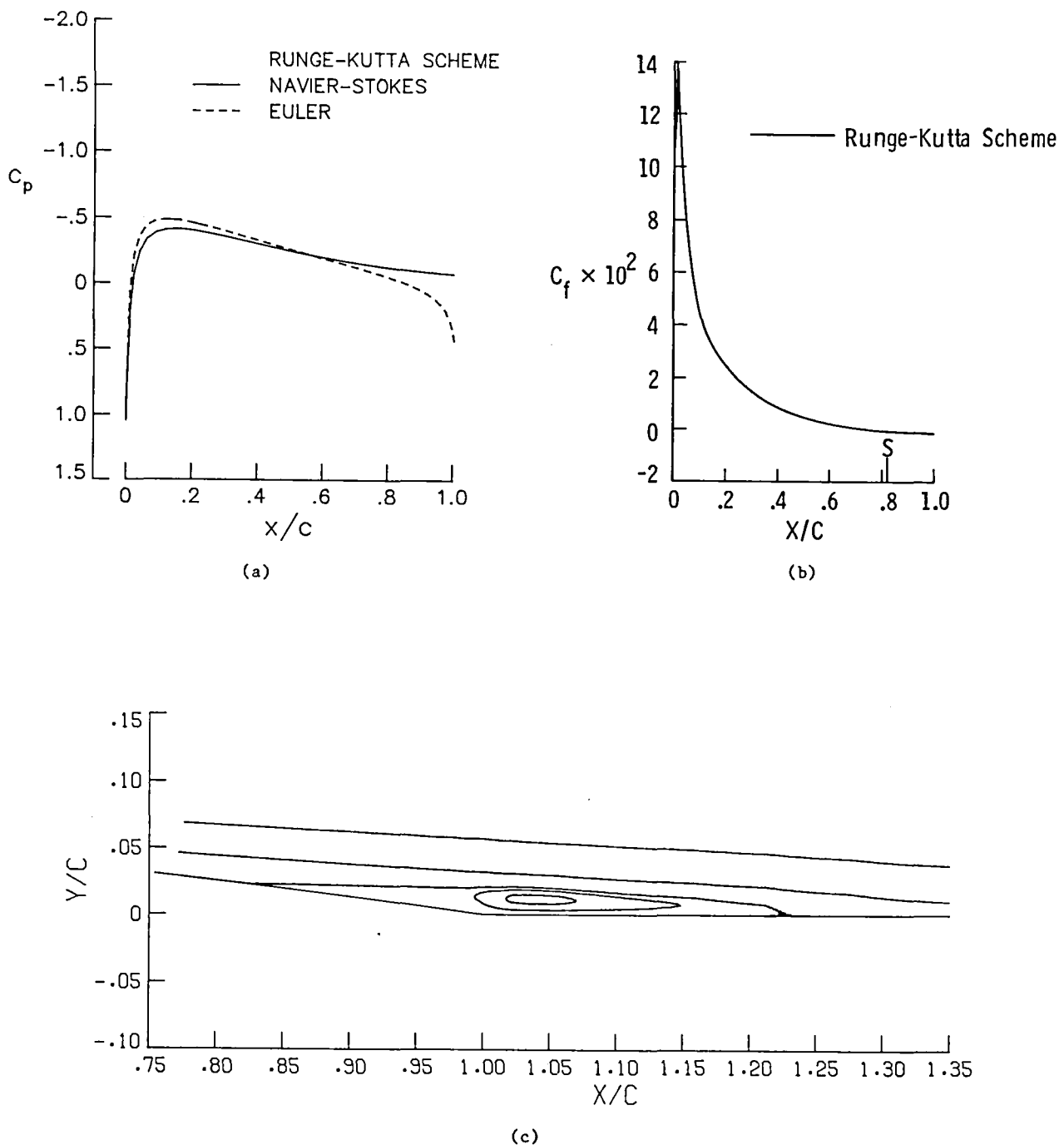


Figure 6. Laminar flow over an NACA 0012 airfoil:

(a) pressure distributions; (b) skin-friction distribution;
(c) streamlines for upper surface at the trailing edge
($M_\infty = 0.5$, $Re_\infty = 5 \times 10^3$).

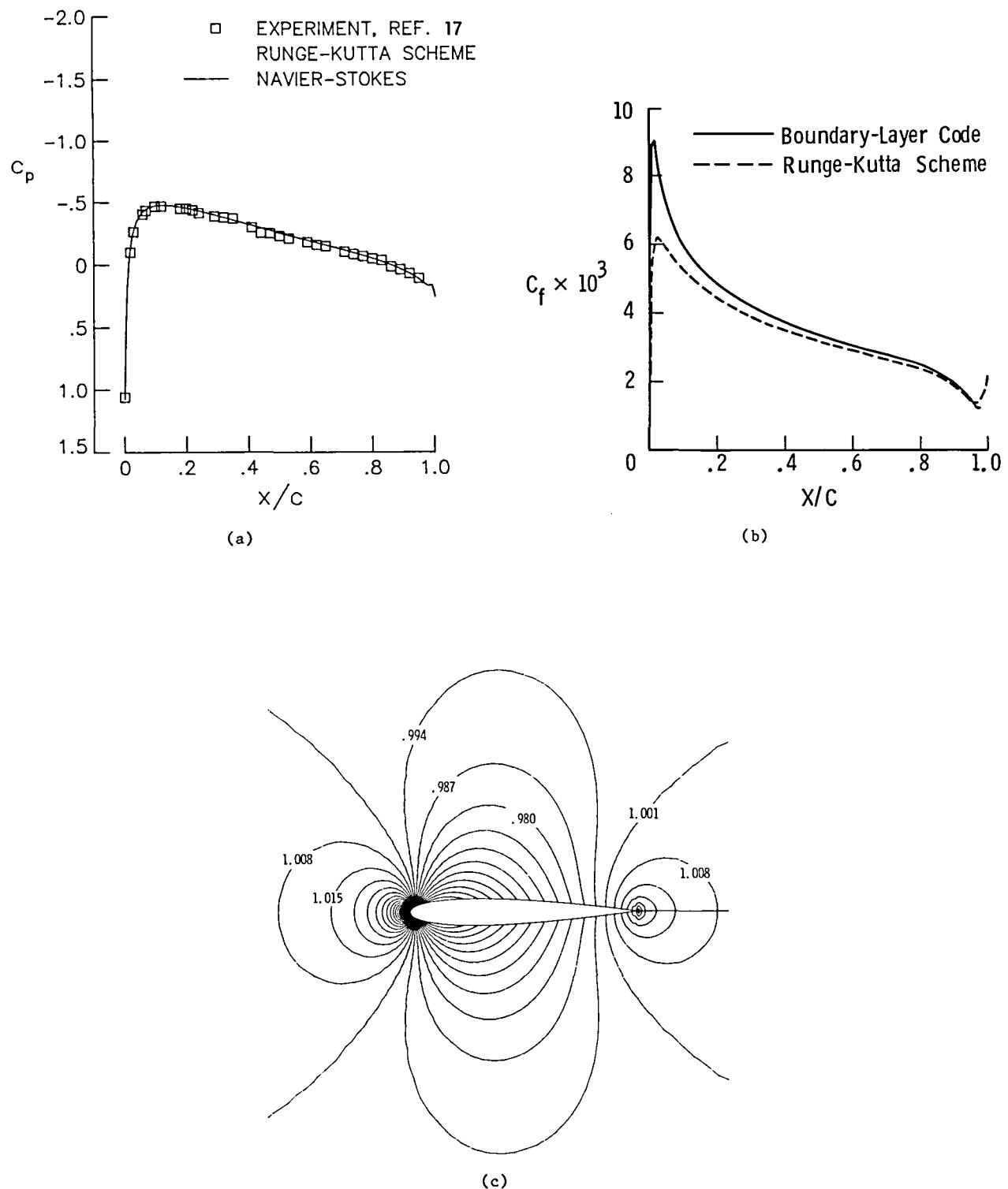


Figure 7. Turbulent flow over an NACA 0012 airfoil:
 (a) pressure distributions; (b) skin friction distributions;
 (c) pressure contours ($M_\infty = 0.5$, $Re_\infty = 2.89 \times 10^6$).

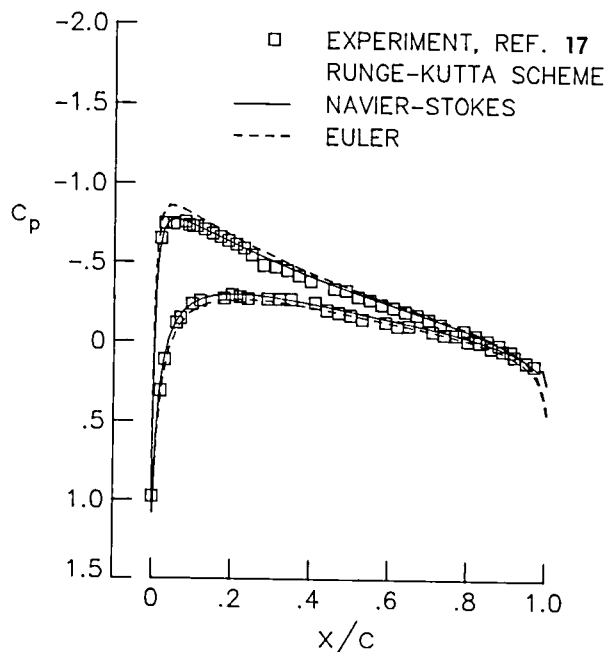


Figure 8. Pressure distributions for flow over an NACA 0012 airfoil at angle of attack ($M_\infty = 0.5$, $Re_\infty = 2.91 \times 10^6$, $\alpha = 1.77^\circ$). Lift coefficient: Experiment - 0.195; Viscous - 0.198; Inviscid - 0.252.

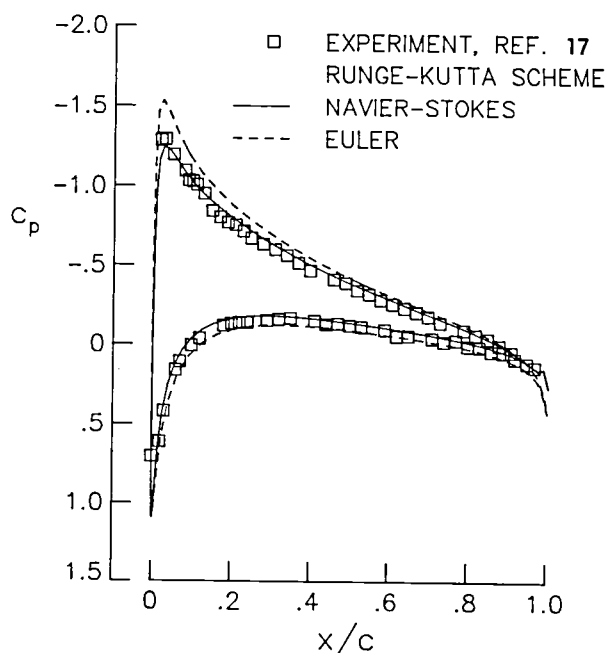
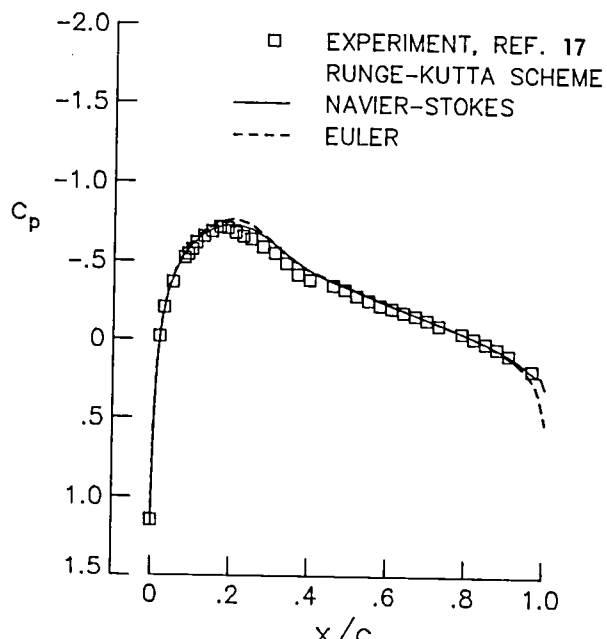
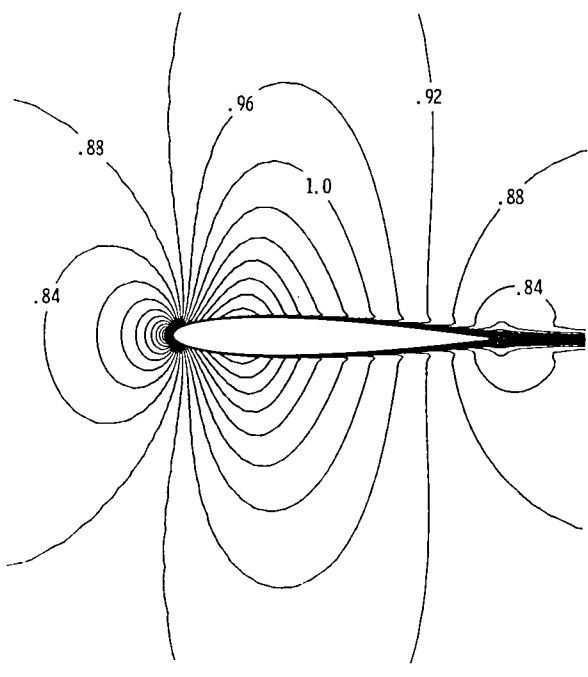


Figure 9. Pressure distributions for flow over an NACA 0012 airfoil at angle of attack ($M_\infty = 0.5$, $Re_\infty = 2.93 \times 10^6$, $\alpha = 3.51^\circ$). Lift coefficient: Experiment - 0.386; Viscous - 0.388; Inviscid - 0.429.



(a)



(b)

Figure 10. Supercritical flow over an NACA 0012 airfoil:
(a) Pressure distributions; (b) Mach number contours
($M_\infty = 0.756$, $Re_\infty = 4.01 \times 10^6$).

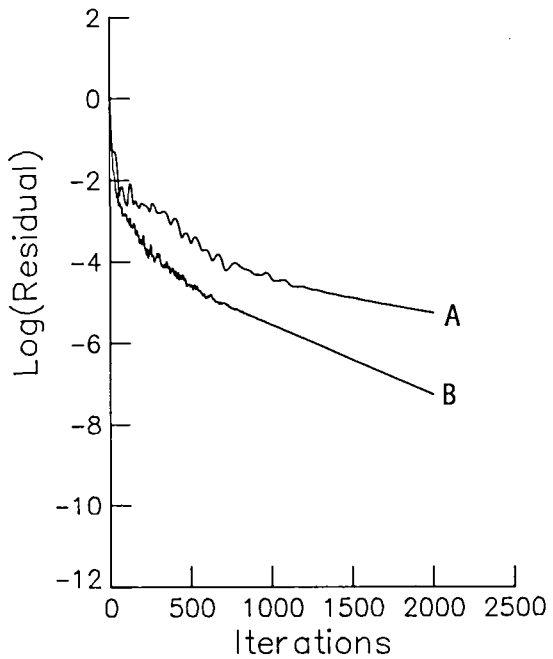


Figure 11. Convergence histories for an NACA 0012 airfoil computation
($M_\infty = 0.5$, $Re_\infty = 5000$, 128×32 cell grid).
A - enthalpy damping; B - enthalpy damping and residual smoothing.

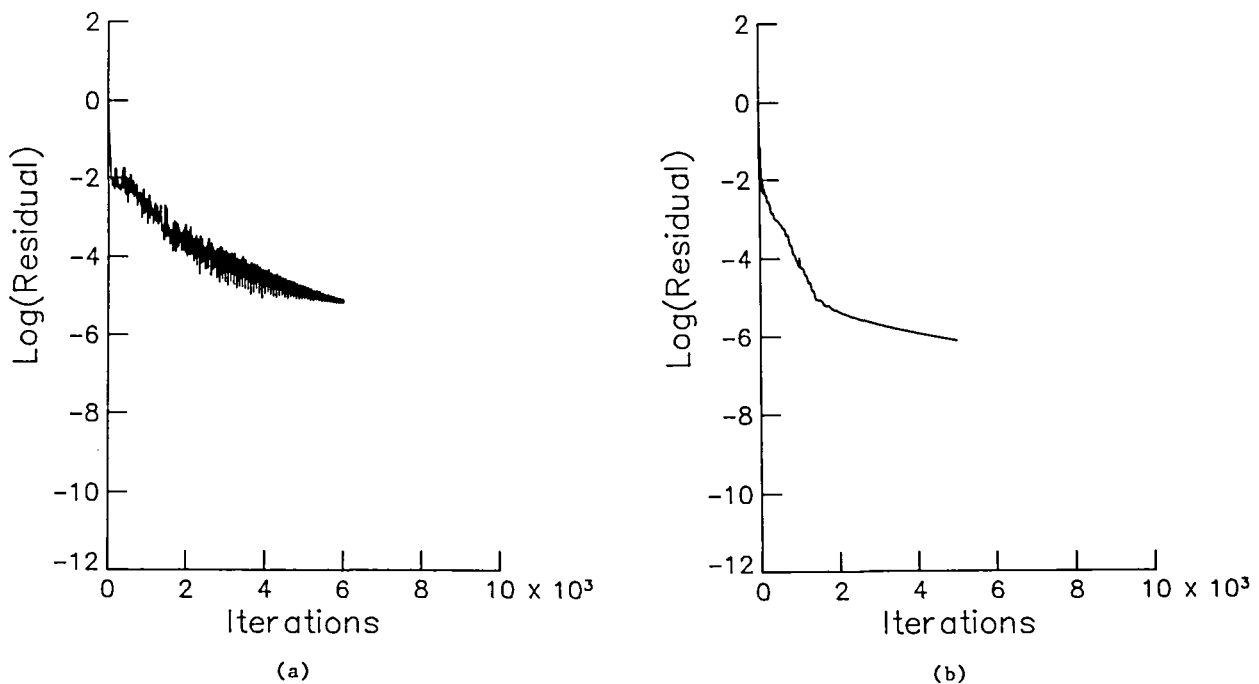


Figure 12. Convergence histories for NACA 0012 airfoil computation
($M_\infty = 0.5$, $Re_\infty = 2.89 \times 10^6$, 120×50 cell grid):
(a) local time-stepping only; (b) enthalpy damping and residual smoothing.

1. Report No. NASA CR-172527 ICASE Report No. 84-62	2. Government Accession No.	3. Recipient's Catalog No.	
4. Title and Subtitle A MULTISTAGE TIME-STEPPING SCHEME FOR THE NAVIER-STOKES EQUATIONS		5. Report Date February 1985	
		6. Performing Organization Code	
7. Author(s) R. C. Swanson and Eli Turkel		8. Performing Organization Report No. 84-62	
9. Performing Organization Name and Address Institute for Computer Applications in Science and Engineering Mail Stop 132C, NASA Langley Research Center Hampton, VA 23665		10. Work Unit No.	
		11. Contract or Grant No. NASI-17070	
		13. Type of Report and Period Covered Contractor Report	
12. Sponsoring Agency Name and Address National Aeronautics and Space Administration Washington, D.C. 20546		14. Sponsoring Agency Code 505-31-83-01	
15. Supplementary Notes Langley Technical Monitor: J. C. South, Jr. Final Report			
16. Abstract <p>A class of explicit multistage time-stepping schemes is used to construct an algorithm for solving the compressible Navier-Stokes equations. Flexibility in treating arbitrary geometries is obtained with a finite-volume formulation. Numerical efficiency is achieved by employing techniques for accelerating convergence to steady state. Computer processing is enhanced through vectorization of the algorithm. The scheme is evaluated by solving laminar and turbulent flows over a flat plate and an NACA 0012 airfoil. Numerical results are compared with theoretical solutions or other numerical solutions and/or experimental data.</p>			
17. Key Words (Suggested by Author(s)) Navier-Stokes, finite volume, Runge-Kutta.		18. Distribution Statement 34 - Fluid Mechanics and Heat Transfer Unclassified - Unlimited	
19. Security Classif. (of this report) Unclassified	20. Security Classif. (of this page) Unclassified	21. No. of Pages 36	22. Price A03

For sale by the National Technical Information Service, Springfield, Virginia 22161

NASA-Langley, 1985



3 1176 00519 3645